FRB 121102 is coincident with a star-forming region in its host galaxy

Bassa, C. G.; Tendulkar, S. P.; Adams, E. A. K.; Maddox, N.; Bogdanov, S.; Bower, G. C.; Burke-Spolaor, S.; Butler, B. J.; Chatterjee, S.; Cordes, J. M.; Hessels, J. W. T.; Kaspi, V. M.; Law, C. J.; Marcote, B.; Paragi, Z.; Ransom, S. M.; Scholz, P.; Spitler, L. G.; Langevelde, H. J. van

Publisher's version / Version de l'éditeur:
https://doi.org/10.3847/2041-8213/aa7a0c
The Astrophysical Journal, 843, 1, p. L8, 2017-07-01

The Astrophysical Journal Letters, 843:L8 (6pp), 2017 July 1 https://doi.org/10.3847/2041-8213/aa7a0c

FRB 121102 Is Coincident with a Star-forming Region in Its Host Galaxy

C. G. Bassa[1], S. P. Tendulkar[2], E. A. K. Adams[1], N. Maddox[1], S. Bogdanov[3], G. C. Bower[4], S. Burke-Spolaor[5,6,7], B. J. Butler[5], S. Chatterjee[8], J. M. Cordes[8], J. W. T. Hessels[1,9], V. M. Kaspi[2], C. J. Law[10], B. Marcote[11], Z. Paragi[11], S. M. Ransom[12], P. Scholz[13], L. G. Spitler[14], and H. J. van Langevelde[11,15]

[1] ASTRON, the Netherlands Institute for Radio Astronomy, Postbus 2, NL-7990 AA Dwingeloo, The Netherlands; bassa@astron.nl
[2] Department of Physics and McGill Space Institute, McGill University, 3600 University Street, Montreal, QC H3A 2T8, Canada
[3] Columbia Astrophysics Laboratory, Columbia University, New York, NY 10027, USA
[4] Academia Sinica Institute of Astronomy and Astrophysics, 645 N. A'ohoku Place, Hilo, HI 96720, USA
[5] National Radio Astronomy Observatory, Socorro, NM 87801, USA
[6] Department of Physics and Astronomy, West Virginia University, Morgantown, WV 26506, USA
[7] Center for Gravitational Waves and Cosmology, West Virginia University, Chestnut Ridge Research Building, Morgantown, WV 26505, USA
[8] Cornell Center for Astrophysics and Planetary Science and Department of Astronomy, Cornell University, Ithaca, NY 14853, USA
[9] Anton Pannekoek Institute for Astronomy, University of Amsterdam, Science Park 904, NL-1098 XH Amsterdam, The Netherlands
[10] Department of Astronomy and Radio Astronomy Lab, University of California, Berkeley, CA 94720, USA
[11] Joint Institute for VLBI ERIC, Postbus 2, NL-7990 AA Dwingeloo, The Netherlands
[12] National Radio Astronomy Observatory, Charlottesville, VA 22903, USA
[13] National Research Council of Canada, Herzberg Astronomy and Astrophysics, Dominion Radio Astrophysical Observatory, P.O. Box 248, Penticton, BC V2A 6J9, Canada
[14] Max-Planck-Institut für Radioastronomie, Auf dem Hügel 69, D-53121 Bonn, Germany
[15] Leiden Observatory, Leiden University, P.O. Box 9513, NL-2300 RA Leiden, The Netherlands
Received 2017 May 22; revised 2017 June 14; accepted 2017 June 16; published 2017 June 27

Abstract

We present optical, near-infrared, and mid-infrared imaging of the host galaxy of FRB 121102 with the Gemini North telescope, the *Hubble Space Telescope*, and the *Spitzer Space Telescope*. The FRB 121102 host galaxy is resolved, revealing a bright star-forming region located in the outskirts of the irregular, low-metallicity dwarf galaxy. The star-forming region has a half-light radius of 0.68 kpc (0.″20), encompassing the projected location of the compact (<0.7 pc), persistent radio source that is associated with FRB 121102. The half-light diameter of the dwarf galaxy is 5–7 kpc, and broadband spectral energy distribution fitting indicates that it has a total stellar mass of $M_\star \sim 10^8\,M_\odot$. The properties of the host galaxy of FRB 121102 are comparable to those of extreme emission line galaxies, also known as hosts to some hydrogen-poor superluminous supernovae and long-duration γ-ray bursts. The projected location of FRB 121102 within the star-forming region supports the proposed connection of FRBs with newly born neutron stars or magnetars.

Key words: galaxies: dwarf – galaxies: star formation – gamma-ray burst: general – supernovae: general

1. Introduction

Over a decade ago, Lorimer et al. (2007) presented the discovery of a millisecond-duration radio transient whose large dispersion measure suggested an extragalactic origin. Since then, the discovery of a population of fast radio burst (FRB) sources (e.g., Thornton et al. 2013; Spitler et al. 2014; Masui et al. 2015) has fueled questions pertaining to both their physical origin and whether they can be used as probes of the intervening (inter-)galactic material. Many theoretical models have been proposed, including those that invoke a cataclysmic event, and those in which repeated bursts from the same source are possible. Regardless, the FRB phenomenon has generated great interest because the short durations and cosmological distances necessarily imply sites of extreme energy density.

The detection of polarization, Faraday rotation, and scintillation in some FRBs has given clues about their origin —in some cases suggesting that they originate from dense and highly magnetized environments like those of a supernova remnant (Masui et al. 2015). The discovery of repeated radio bursts from FRB 121102 immediately ruled out cataclysmic progenitor models—at least for this particular source (Scholz et al. 2016; Spitler et al. 2016). However, deep campaigns to search for repeat bursts from other known FRB positions have thus far detected no other repeaters (Petroff et al. 2015), suggesting perhaps that there is more than one class of FRB progenitor within the sample of 22 known sources (Petroff et al. 2016).

In a practical sense, the repetition of FRB 121102 greatly facilitates follow-up and precision localization. Monitoring of the FRB 121102 field using the Very Large Array in a fast-dump recording mode (Law et al. 2015) led to a sub-arcsecond localization of the radio bursts and the discovery of the optical host galaxy and a persistent radio counterpart (Chatterjee et al. 2017). Very long baseline interferometry (VLBI) using Arecibo and the European VLBI Network (EVN) constrained the source of the FRB 121102 bursts and the position of the persistent radio source to be within 12 mas from each other (Marcote et al. 2017). This led to the conclusion that the source of the FRB 121102 bursts has a direct physical link to the source of the persistent radio emission, e.g., the burst source could be embedded in a radio-bright nebula. Spectroscopy of the optical host galaxy identified it as a low-mass, low-metallicity dwarf galaxy at redshift $z = 0.193$ (Tendulkar et al. 2017), constituting the first unambiguous identification of an FRB host and its precise distance.

A tantalizing clue resulting from the identification of the host galaxy of FRB 121102 is that similar dwarf galaxies are known to host some long-duration γ-ray bursts (LGRBs; Modjaz et al. 2008) and hydrogen-poor superluminous supernovae (SLSN-I; Lunnan et al. 2014). This could suggest an evolutionary link, in

which the sources of FRB events are born at the times of LGRBs and SLSN-I, with FRBs originating from young neutron stars or magnetars resulting from these explosions (Piro 2016; Beloborodov 2017; Kashiyama & Murase 2017; Metzger et al. 2017).

In this Letter, we present multi-band optical and infrared (IR) imaging of the host galaxy of FRB 121102 with the Gemini North telescope, the *Hubble Space Telescope* (*HST*), and the *Spitzer Space Telescope*. Results from these observations improve upon the properties of the FRB 121102 host galaxy that we presented in Tendulkar et al. (2017). In Section 2, we report on the observations and analysis. The morphology, environment, and properties of the host galaxy are presented in Section 3. We discuss our results in Section 4.

2. Observations and Analysis

2.1. Hubble Space Telescope

We acquired *HST* imaging observations of the FRB 121102 field on 2017 February 23 using the WFC3/UVIS and WFC3/IR cameras (data sets IDE601010, IDE601020, IDE601030, and IDE601040). We chose the F763M and F845M filters to cover the redshifted Hα emission line and the continuum redward of Hα. In the near-IR we used the F110W and F160W filters, which are comparable to the J (1.1 μm) and H (1.6 μm) bands. The exposure times were 1940 s (F763M), 2560 s (F845M), 1797 s (F110W), and 1197 s (F160W). We used 4-point dither patterns appropriate for the UVIS and IR cameras to improve the sampling of the point-spread function (PSF) and to mitigate cosmic rays and hot pixel issues.

The data were processed through STScI's `drizzlepac` package (Gonzaga et al. 2012; Avila et al. 2015) to drizzle and mosaic the images. The final resolution was chosen to include 2.5 drizzled pixels in the FWHM of the PSF appropriate for each wavelength. The images were combined with optimal weighting proportional to inverse of the pixel variance (i.e., `IVM` weighting). The `drizzlepac` pipeline also produced pixel weight images for each filter. Each drizzled and mosaicked image was astrometrically matched to the *Gaia* DR1 catalog (Gaia Collaboration et al. 2016). The rms residuals of the astrometric calibration were 8–9 mas for each image, using of order 50 (80) *Gaia* standards for the IR (UVIS) images. We performed photometry on the reduced images using the `Source Extractor` package (Bertin & Arnouts 1996), generating isophotal aperture magnitudes, corrected for blending. We used AB magnitude zero-points for each filter as defined by STScI.[16] The `Source Extractor` catalogs were then merged with photometry in other filters.

2.2. Spitzer Space Telescope

We acquired *Spitzer* IRAC (Fazio et al. 2004) observations of FRB 121102 on 2017 January 4 with the 3.6 and 4.5 μm bands (Obs ID 62322432). The observation was split into 100 dithered exposures of 100 s for each band. The data were processed through the `MOPEX` software using the mosaicking and the multi-frame point-source extraction pipeline. We used the detected source catalog from the *HST* F160W image as input to the pixel response function fitting photometry and source extraction routine. The positions of the sources were held fixed while the fluxes were fit.

[16] http://www.stsci.edu/hst/wfc3/analysis/uvis_zpts for UVIS and http://www.stsci.edu/hst/wfc3/ir_phot_zpt for IR.

2.3. Gemini

Imaging observations of the host galaxy of FRB 121102 were obtained with the Gemini Multi-Object Spectrograph (GMOS) on the 8 m Gemini North telescope atop Mauna Kea, Hawai'i (program GN-2016B-DD-2). On 2016 December 29 we obtained deep exposures in g' (12×300 s) and in r' (6×250 s). The conditions during these observations were photometric, with the seeing varying between 0.″6 and 0.″8. The GMOS images were read out with 2×2 binning, yielding a pixel scale of 0.″146. These observations are in addition to the deep r', i', and z' imaging presented in Tendulkar et al. (2017), and were bias-corrected, flat-fielded, registered, and co-added in an identical manner.

All co-added GMOS images were astrometrically calibrated against *Gaia* standards, using 40–50 unblended stars and yielding rms residuals of 9–10 mas. Instrumental magnitudes of objects on the co-added GMOS images were determined through isophotal aperture photometry with `Source Extractor` (Bertin & Arnouts 1996). The instrumental magnitudes were calibrated directly to the AB system with photometry from Pan-STARRS 1 DR1 (Chambers et al. 2016; Magnier et al. 2016). Due to the similarity between the GMOS and Pan-STARRS filters, no color terms were required, and we fitted only zero-point offsets.

3. Results

The drizzled WFC3 images obtained in the F110W and F160W bands show that the object identified by Chatterjee et al. (2017) and Tendulkar et al. (2017) as the host galaxy of FRB 121102 consists of a compact and bright knot, offset from diffuse emission (Figure 1). We obtain isophotal aperture magnitudes of the host galaxy (both the knot and diffuse emission) of $m_{\rm F110W} = 23.675(12)$ and $m_{\rm F160W} = 23.31(3)$ in the AB system. In the lower-resolution GMOS images, these two components are blended, yielding isophotal aperture magnitudes (AB system) of $g' = 25.85(12)$, $r' = 25.46(14)$, $i' = 24.75(9)$, and $z' = 24.30(13)$. In the *Spitzer* images, the host galaxy flux was measured to be 1.03 ± 0.19 μJy and <0.9 μJy (6σ) in the 3.6 μm and 4.5 μm bands, respectively.

Our r'- and i'-band magnitudes for the host galaxy of FRB 121102 are fainter by 0.4 and 0.9 mag compared to what we obtained in Tendulkar et al. (2017). We attribute this difference to an error in the aperture photometry reported in Tendulkar et al. (2017). As a result of the overestimated brightness of the host, the WFC3 UVIS exposure times were underestimated, unfortunately leading to low signal-to-noise ratios in the F763M and F845M images. Only the knot is detected at 5σ in the F763M image. We note though that the flux scale of the GMOS spectrum of the FRB 121102 host galaxy of Tendulkar et al. (2017) is is correct, as this was scaled to the i'-band magnitude of the reference star, which was not affected by the error in the aperture photometry.

The high spatial resolution of the F110W and F160W images allows us to confirm our hypothesis we suggested in Tendulkar et al. (2017); we identify the knot as a star-forming region responsible for the observed emission line spectrum, while the diffuse emission corresponds to the underlying stellar population of the FRB 121102 host galaxy. The flux from the

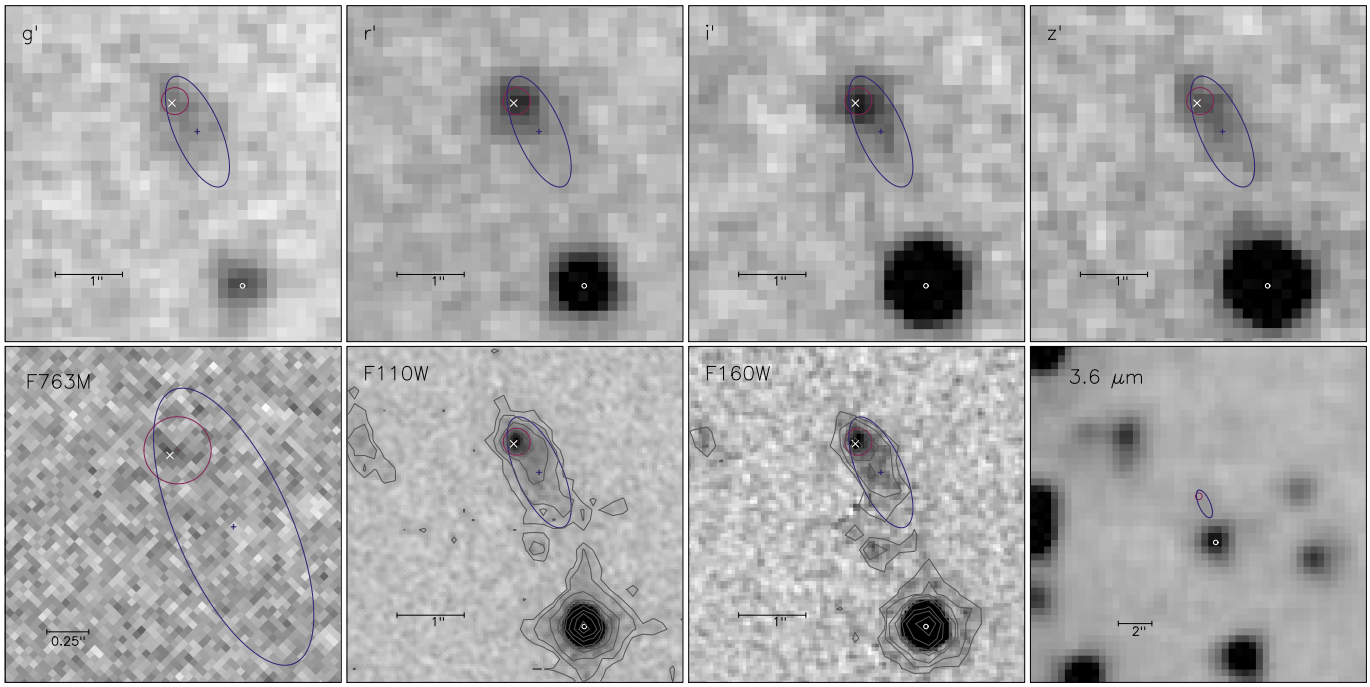

Figure 1. Subsections of the GMOS g', r', i', and z' images (top row, all $5'' \times 5''$), and of the *HST*/WFC3 F763M (redshifted Hα, $2'' \times 2''$), F110W (J), and F160W (H) images (both $5'' \times 5''$) and the *Spitzer* 3.6 μm image ($20'' \times 20''$, bottom row). North is to the top and east to the left. The GMOS images have been smoothed with a Gaussian with a width of $0\farcs1$. We fit the centroid and half-light radius of both the bright knot and extended diffusing emission using the F110W image. These centroids and half-light radii are denoted by the red circle and the large blue ellipse, respectively, in each frame. Contours are overlaid on the F110W and F160W images to indicate the extent of the host galaxy. The white circle denotes the position of the reference star while the white cross in the GMOS and *HST*/WFC3 images denotes the location of FRB 121102 and the associated persistent radio source by Marcote et al. (2017) at 5 GHz (0.6 mas uncertainty, smaller than the symbol).

star-forming knot in the r' and i' bands is dominated by the bright emission lines of Hα, Hβ, [O III] λ4959, and [O III] λ5007. As a result, the position and extent of the host galaxy, as we determined in Tendulkar et al. (2017), reflects the differing contributions of the star-forming knot compared to the rest of the host galaxy. The emission from the knot in the F110W and F160W bands is expected to contain emission lines of [S III] 0.907 μm, [S III] 0.953 μm, He I 1.083 μm, Paδ, Paγ, and Paβ (Martins et al. 2013; see also Figure 2), explaining its brightness compared to the diffuse emission.

In the remainder of the Letter, we use cosmological parameters from Planck Collaboration et al. (2016) as implemented in `astropy.cosmology` (Astropy Collaboration et al. 2013).

3.1. Morphology

We determine the position and extent of the star-forming complex (the knot) and the underlying stellar population in the drizzled F110W image by modeling and jointly fitting them as two-dimensional Gaussian or Moffat (Moffat 1969) profiles. We find that the ellipticity of the knot is close to unity, so we fit it with a circular Moffat function instead. The knot has a radius of $\sigma = 0\farcs24(1)$, significantly larger than the radius of the stellar PSF, for which a Moffat fit yields radii of $\sigma = 0\farcs165$. The diffuse emission appears irregular in the near-IR images (Figure 1). For simplicity, we fit the stellar population with a Gaussian profile, which yields a semimajor axis of $\sigma_a = 0\farcs66(3)$ with $b/a = 0.40(2)$, and a position angle of 66°. Transferring the position of the knot and the diffuse emission to the F160W image and keeping the positions fixed, we find comparable results for the position and size of the star-forming region. The diffuse emission prefers a larger semimajor axis of $\sigma_a = 0\farcs85(3)$ and a smaller ellipticity of $b/a = 0.36(2)$.

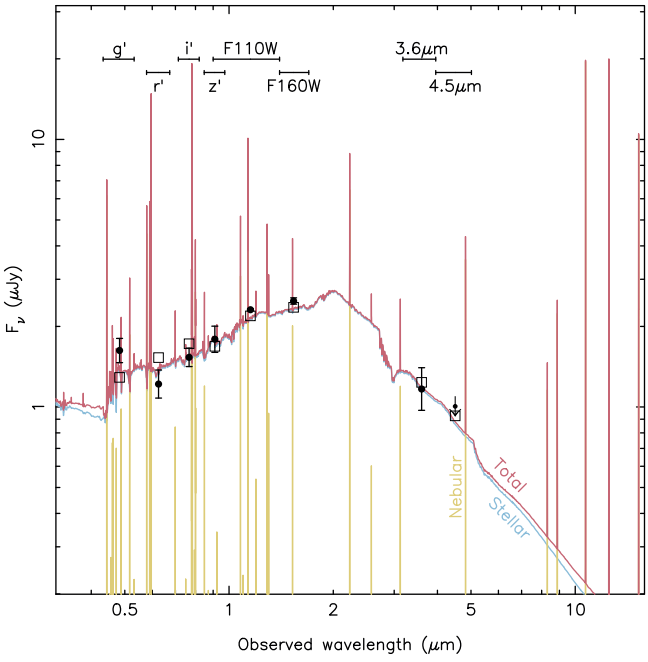

Figure 2. Spectral energy distribution (SED) for the host galaxy of FRB 121102. Photometric measurements or upper limits from Gemini, *HST*, and *Spitzer* are indicated with black dots or a downward arrow, with the respective bandpasses indicated at the top. The stellar and nebular (from star formation) components making up the total emission of the SED fit are shown in different colors. The predicted model fluxes are shown with open squares.

We estimate the intrinsic radius of the knot as the quadratic difference of the observed radius and that of the stellar PSF.

The resulting half-light radius corresponds to an HWHM (Gaussian HWHM, 1.1774σ) of $0\farcs20(1)$. At a redshift of $z = 0.193$, an angle of $1''$ corresponds to a projected distance of 3.31 kpc, hence the half-light radius is 0.68(3) kpc. Under the assumption that the diffuse emission due to the underlying stellar population can be represented by a Gaussian (which, given the irregular nature of dwarf galaxies may not be valid), the knot is located $0\farcs57$ (1.9 kpc) from the nominal centroid of the diffuse emission, which itself has a half-light diameter (Gaussian FWHM) between $1\farcs5$ and $2\farcs0$ (5 to 7 kpc). The higher spatial resolution and greater depth of the *HST* observations improve upon the $\lesssim$4 kpc diameter we estimated in Tendulkar et al. (2017). The centroid of the knot, as measured in the drizzled F110W image, is located at $\alpha_{\rm J2000} = 05^{\rm h}31^{\rm m}58\fs6980(8)$, $\delta_{\rm J2000} = +33°08'52\farcs671(10)$. This position is consistent with that determined from the 5σ detection of the knot in the F763M image, as well as the F160W image. The milliarcsecond-precision location of the persistent radio source at 5 GHz with the EVN, and with it the source of the radio bursts (Marcote et al. 2017), is offset from the center of the star-forming region by $0\farcs055(14)$ or 0.18(5) kpc, but located within the nominal half-light radius of the star-forming region. The nearby reference star is located at $\alpha_{\rm J2000} = 05^{\rm h}31^{\rm m}58\fs6180(8)$, $\delta_{\rm J2000} = +33°08'49\farcs831(1)$.

3.2. Spectral Energy Distribution (SED) Fitting

We use our multi-wavelength photometry to model the SED of the host galaxy of FRB 121102 with the `CIGALE`[17] software (Noll et al. 2009; Serra et al. 2011). We fit an underlying older stellar population with a recent burst of star formation. Figure 2 shows the resulting SED. One of the largest sources of uncertainties is the foreground Galactic extinction. We used both the Schlegel et al. (1998) and Schlafly & Finkbeiner (2011) foreground extinction values and found no appreciable differences in our best-fitting SED and derived parameters, and we report results using the Schlegel et al. (1998) Galactic extinction correction. We find that the host has negligible internal dust extinction, as expected for a metal-poor dwarf galaxy. Our best value for the recent star formation (averaged over the last 10 Myr) is $0.13(4)\,M_\odot\,{\rm yr}^{-1}$. This value does not fully capture the current star formation as measured directly from the Hα luminosity determined from spectroscopy ($0.23\,M_\odot\,{\rm yr}^{-1}$ from Tendulkar et al. 2017, with no internal extinction correction), but is roughly consistent. We find a stellar mass of $M_\star = (1.3 \pm 0.4) \times 10^8\,M_\odot$, which corresponds to a mass-to-light ratio of $\sim$0.6 in the r' band. The stellar mass is dominated by the older stellar population and so is insensitive to the exact details of the recent star formation. However, we note that the inherent uncertainties in determining the stellar mass from SED fitting are at least a factor of two (Pforr et al. 2012). The stellar mass is somewhat larger, but is consistent with the $\sim(4\text{–}7) \times 10^7\,M_\odot$ we estimated in Tendulkar et al. (2017).

3.3. Metallicity

In Tendulkar et al. (2017) we placed rough constraints on the metallicity of the host galaxy using the measured emission lines. These constraints suffered from the fact that [O II] λ3727 and [O III] λ4363 were outside our wavelength coverage. Here we use the `HII-CHI-mistry`[18] software (Pérez-Montero 2014) to obtain a more robust constraint on the metallicity of the host galaxy. This software uses grids of photoionization models to derive abundances consistent with the direct method, or T_e method, wherein the electron temperature of the gas is constrained by measuring the ratio between the [O III] λ4363 and [O III] λ5007 lines. By assuming empirical laws between O/H, N/O, and the ionization parameter $\log U$, it provides reasonable metallicities even when the temperature sensitive [O III] λ4363 line is not present, as is the case for our spectrum. Using either the 3σ upper limit for [N II] λ6584 or a tentative $\sim1.7\sigma$ detection, we find $12 + \log_{10}([{\rm O/H}]) = 8.0 \pm 0.1$. While there are inherent uncertainties in the metallicity of the host galaxy without the measurement of more lines, we can confirm it is a low-metallicity galaxy.

3.4. Star Formation Rate (SFR)

In Tendulkar et al. (2017), we use the Galactic extinction-corrected Hα emission line flux to estimate an SFR of 0.23–0.4 $M_\odot\,{\rm yr}^{-1}$, with the lower value uncorrected for internal extinction and the upper value with a correction applied. Due to the negligible dust content of low-metallicity dwarf galaxies, the internal extinction in the host galaxy of FRB 121102 is low (Kokubo et al. 2017), and thus we adopt the uncorrected Hα SFR of $0.23\,M_\odot\,{\rm yr}^{-1}$ as the best estimate. This value is also more in line with the lower SFR derived from the SED fitting of $0.12\,M_\odot\,{\rm yr}^{-1}$.

This star formation will also be observable in the radio continuum, which has the advantage of being unaffected by dust obscuration from the Galactic plane. Using the relation between SFR and 1.4 GHz radio luminosity from Murphy et al. (2011), the Hα-derived SFR corresponds to 3 μJy. From Chatterjee et al. (2017), the VLA 1.4 GHz flux is 250 ± 39 μJy; however, this includes flux not only from star formation, but also from the persistent radio source that is embedded within the star-forming region. The *HST* imaging shows the star-forming region confined to a region of $\sim0\farcs2$ in radius, scales that are resolved out in the EVN observations presented in Marcote et al. (2017). These EVN observations show that the persistent radio source flux at 1.7 GHz varies between 168 and 220 μJy, with flux calibration uncertainties of the order of 20%. The VLA and EVN fluxes are compatible within a few μJy of flux associated with star formation.

The star-forming knot is barely resolved in the *HST* images, so we have no detailed information about its internal structure. We expect the star-forming complex to be composed of a number of individual, unresolved, star-forming regions. Giant molecular clouds found in the LMC (Hughes et al. 2010) and interacting Antennae galaxies (Zaragoza-Cardiel et al. 2014) reach 100 pc or more in size. A few of such GMCs in close proximity to each other would be sufficient to produce such a star-forming region.

3.5. Environment of the FRB 121102 Host Galaxy

We have made a crude estimate of the environment of the FRB host galaxy, using the *HST* F110W (*J*-band) image. First we count the number of objects within a fixed-radius aperture of $15\farcs5$, corresponding to a radius of 50 kpc at the redshift of the host galaxy, centered on the location of the FRB. This is

[17] Available at http://cigale.lam.fr/.

[18] Available at http://www.iaa.es/~epm/HII-CHI-mistry.html.

large enough to encompass the immediate and extended environment of the FRB host galaxy.

As galaxy clustering strength is a function of galaxy mass, with more massive galaxies being more strongly clustered than low-mass galaxies (Zehavi et al. 2002), we select other objects in the image within ± 0.15 mag of the FRB host magnitude, but outside the FRB host aperture. At these faint magnitudes, the objects will either be dwarf galaxies like the FRB host (albeit at unknown redshifts), or very high redshift, more massive galaxies. We place the same $15\farcs5$ aperture around each of these magnitude-matched galaxies and count the number of objects to use as control regions. No attempt to remove foreground stars has been made, as it is assumed to be qualitatively the same for every aperture and will thus cancel out.

For the *HST* J-band image, there are 30 objects within the $15\farcs5$ aperture to $J \leqslant 26.5$ for both the FRB and 31 control regions, but their distribution in radius is different. From the cumulative number counts, the FRB region is more centrally concentrated, with 18 objects within $10''$ compared to a median value of 14 ± 4 in the control regions. Beyond this radius, the cumulative number count distributions are the same for the FRB and control regions. Thus, on small (<50 kpc) scales, there is a marginal hint of an overdensity centered on the FRB host galaxy. On larger scales, the environment is typical of other objects with the same apparent magnitude. The irregular morphology of the host galaxy is consistent with past or ongoing interactions.

4. Discussion and Conclusions

We present optical, near-IR, and mid-IR imaging that improves on the ground-based imaging presented in Tendulkar et al. (2017) and resolves the host galaxy of FRB 121102, revealing a bright knot of star formation located in the outskirts of an irregular (5–7 kpc half-light diameter), low-mass ($M_\star \sim 10^8\,M_\odot$), low-metallicity ($12 + \log_{10}([\mathrm{O/H}]) = 8.0$) dwarf galaxy. The persistent radio source that is coincident with the FRB (Chatterjee et al. 2017; Marcote et al. 2017) is located within the 0.68 kpc half-light radius of the star-forming region. Recent high spatial resolution Hα observations confirm the coincidence of FRB 121102 with the star-forming region in its host galaxy, and yield similar estimates of the size of the star-forming region and the offset of the FRB with its centroid (Kokubo et al. 2017).

The separation of the underlying stellar population of the FRB 121102 host galaxy from the star-forming region allows us to update our estimate of the dispersion measure (DM) that can be attributed to the Hα emitting gas. Following our derivation in Section 4.3 of Tendulkar et al. (2017), the smaller size of the star-forming region increases the Hα surface density by a factor of 3.3. As a result, the maximum host DM depth increases by a factor of 1.8 to $\mathrm{DM_{host}} \lesssim 589\,\mathrm{pc\,cm^{-3}}\ L_{\mathrm{kpc}}^{1/2}$ (with $L_{\mathrm{FRB}} \leqslant L_{\mathrm{kpc}}$), consistent with the estimate derived by Kokubo et al. (2017).

As we already noted in Tendulkar et al. (2017), with its low mass, low metallicity, and strong emission lines, the host galaxy of FRB 121102 shows many similarities with a class of star-forming galaxies known as extreme emission line galaxies (EELGs; Atek et al. 2011; van der Wel et al. 2011). The *HST* imaging reveals that the morphology of the host galaxy, an underlying disturbed stellar population dominated by a compact star-forming region, is consistent with the cometary or tadpole shapes of EELGs (Amorín et al. 2015). The one possible contrasting metric is that we find the FRB host to be in a region of average or slightly high density, whereas EELGs are generally found in underdensities (Amorín et al. 2015).

The EELG galaxy classification encompasses several subclasses of galaxies found in the literature. At the low-mass end of the EELG population are compact and ultracompact blue dwarf galaxies (CBDs, UCBDs; Thuan & Martin 1981; Corbin et al. 2006). *HST* imaging of a sample of very low redshift UCBDs reveals remarkable similarities to the FRB host galaxy, showing objects with diffuse, irregular structure, punctuated by compact regions of intense star formation spanning tens to hundreds of parsecs, offset from the galaxy center (Corbin et al. 2006). We note that the specific SFR (sSFR; SFR divided by stellar mass) and metallicity of the FRB host are comparable to those of high-redshift ($z \sim 5$) Lyman break galaxies (LBGs; Greis et al. 2016). This indicates that galaxies similar to the repeating FRB host were common in the early universe, so we might expect similar FRBs at higher redshifts.

Of particular interest are the hydrogen-poor superluminous supernovae (SLSN-I), which preferably occur in EELGs (Leloudas et al. 2015; Perley et al. 2016). There is some disagreement as to whether the SLSN-I hosts are also drawn from the same galaxy pool as the hosts of long-duration γ-ray bursts (LGRBs), with some authors finding the hosts similar (Lunnan et al. 2014) and others finding differences (Angus et al. 2016). In general, the half-light radius and SFR of the knot appears more in line with those of SLSN-I than perhaps LGRBs, as the latter tend to be larger in size and have higher star formation (Lunnan et al. 2015; Angus et al. 2016).

The locations of SLSN-I are found to trace the UV light of their host galaxies (Lunnan et al. 2015), though less so than LGRBs, which strongly prefer the bright, inner regions of their hosts (Blanchard et al. 2016). The coincidence of FRB 121102 with the star formation complex, which is the brightest part of its host galaxy, further strengthens the resemblance between FRBs and SLSN-I/LGRBs. It is not yet clear whether the resemblance is one of low-metallicity star-forming environment or from the sources born from that environment. Regardless, this observed coincidence is supported by models of magnetar birth (Kasen & Bildsten 2010; Woosley 2010), which are believed to be born in the collapse of massive stars. This could suggest an evolutionary link, in which neutron stars or magnetars are born as LGRB or SLSN-I and evolve into FRB-emitting sources (Piro 2016; Beloborodov 2017; Kashiyama & Murase 2017; Metzger et al. 2017; Omand et al. 2017). Volumetric rate estimates of star-forming dwarf galaxies, along with SLSN-I, LGRB, and FRB rates by Nicholl et al. (2017) and Law et al. (2017), indicate broad consistency.

The coincidence of FRB 121102 with a star-forming region —in a host galaxy that is similar in type to those preferentially hosting SLSN-I and LGRBs—suggests that targeted searches for radio bursts or compact persistent radio counterparts, similar to that of FRB 121102, can be a valuable new approach to complement ongoing, wide-field searches for FRBs. The discovery of even a single FRB source in such a targeted search would greatly strengthen the evolutionary connection already suggested by FRB 121102.

Support for *HST* program GO-14890 was provided by NASA through a grant from the Space Telescope Science Institute, which is operated by the Association of Universities for Research in

Astronomy, Inc., under NASA contract NAS 5-26555. This work is based on observations obtained at the Gemini Observatory (GN-2016B-DD-2), which is operated by the Association of Universities for Research in Astronomy, Inc., under a cooperative agreement with the NSF on behalf of the Gemini partnership: the National Science Foundation (United States), the National Research Council (Canada), CONICYT (Chile), Ministerio de Ciencia, Tecnología e Innovación Productiva (Argentina), and Ministério da Ciência, Tecnologia e Inovação (Brazil). This work is also based on observations made with the *Spitzer Space Telescope*, which is operated by the Jet Propulsion Laboratory, California Institute of Technology under a contract with NASA.

C.G.B. and J.W.T.H. acknowledge support from the European Research Council under the European Union's Seventh Framework Programme (FP/2007-2013)/ERC Grant Agreement No. 337062 (DRAGNET; PI Hessels). S.P.T. acknowledges support from the McGill Astrophysics Fellowship. E.A.K.A. is supported by TOP1EW.14.105, which is financed by the Netherlands Organisation for Scientific Research (NWO). J.W.T.H. acknowledges funding from an NWO Vidi fellowship. L.G.S. gratefully acknowledges support from the ERC Starting Grant BEACON under contract No. 279702 and the Max Planck Society. B.M. acknowledges support by the Spanish Ministerio de Economía y Competitividad (MINECO) under grants AYA2016-76012-C3-1-P and MDM-2014-0369 of ICCUB (Unidad de Excelencia "María de Maeztu"). This work has been supported by NSF award #1458952.

Facilities: Gemini:Gillett, *HST*, *Spitzer*.

Software: Source Extractor, DrizzlePac, IRAF, MOPEX, Astropy, ESO-MIDAS.

References

Amorín, R., Pérez-Montero, E., Contini, T., et al. 2015, A&A, 578, A105
Angus, C. R., Levan, A. J., Perley, D. A., et al. 2016, MNRAS, 458, 84
Astropy Collaboration, Robitaille, T. P., Tollerud, E. J., et al. 2013, A&A, 558, A33
Atek, H., Siana, B., Scarlata, C., et al. 2011, ApJ, 743, 121
Avila, R. J., Hack, W., Cara, M., et al. 2015, in ASP Conf. Ser. 495, Astronomical Data Analysis Software an Systems XXIV (ADASS XXIV), ed. A. R. Taylor & E. Rosolowsky (San Francisco, CA: ASP), 281
Beloborodov, A. M. 2017, ApJL, in press (arXiv:1702.08644)
Bertin, E., & Arnouts, S. 1996, A&AS, 117, 393
Blanchard, P. K., Berger, E., & Fong, W.-f. 2016, ApJ, 817, 144
Chambers, K. C., Magnier, E. A., Metcalfe, N., et al. 2016, arXiv:1612.05560
Chatterjee, S., Law, C. J., Wharton, R. S., et al. 2017, Natur, 541, 58
Corbin, M. R., Vacca, W. D., Cid Fernandes, R., et al. 2006, ApJ, 651, 861
Fazio, G. G., Hora, J. L., Allen, L. E., et al. 2004, ApJS, 154, 10
Gaia Collaboration, Brown, A. G. A., Vallenari, A., et al. 2016, A&A, 595, A2
Gonzaga, S., Hack, W., Fruchter, A., & Mack, J. 2012, The DrizzlePac Handbook (Baltimore, MD: STScI)
Greis, S. M. L., Stanway, E. R., Davies, L. J. M., & Levan, A. J. 2016, MNRAS, 459, 2591
Hughes, A., Wong, T., Ott, J., et al. 2010, MNRAS, 406, 2065
Kasen, D., & Bildsten, L. 2010, ApJ, 717, 245
Kashiyama, K., & Murase, K. 2017, ApJL, 839, L3
Kokubo, M., Mitsuda, K., Sugai, H., et al. 2017, ApJ, in press (arXiv:1705.04693)
Law, C. J., Abruzzo, M. W., Bassa, C. G., et al. 2017, arXiv:1705.07553
Law, C. J., Bower, G. C., Burke-Spolaor, S., et al. 2015, ApJ, 807, 16
Leloudas, G., Schulze, S., Krühler, T., et al. 2015, MNRAS, 449, 917
Lorimer, D. R., Bailes, M., McLaughlin, M. A., Narkevic, D. J., & Crawford, F. 2007, Sci, 318, 777
Lunnan, R., Chornock, R., Berger, E., et al. 2014, ApJ, 787, 138
Lunnan, R., Chornock, R., Berger, E., et al. 2015, ApJ, 804, 90
Magnier, E. A., Schlafly, E. F., Finkbeiner, D. P., et al. 2016, arXiv:1612.05242
Marcote, B., Paragi, Z., Hessels, J. W. T., et al. 2017, ApJL, 834, L8
Martins, L. P., Rodríguez-Ardila, A., Diniz, S., Gruenwald, R., & de Souza, R. 2013, MNRAS, 431, 1823
Masui, K., Lin, H.-H., Sievers, J., et al. 2015, Natur, 528, 523
Metzger, B. D., Berger, E., & Margalit, B. 2017, ApJ, 841, 14
Modjaz, M., Kewley, L., Kirshner, R. P., et al. 2008, AJ, 135, 1136
Moffat, A. F. J. 1969, A&A, 3, 455
Murphy, E. J., Condon, J. J., Schinnerer, E., et al. 2011, ApJ, 737, 67
Nicholl, M., Williams, P. K. G., Berger, E., et al. 2017, ApJ, submitted (arXiv:1704.00022)
Noll, S., Burgarella, D., Giovannoli, E., et al. 2009, A&A, 507, 1793
Omand, C. M. B., Kashiyama, K., & Murase, K. 2017, arXiv:1704.00456
Pérez-Montero, E. 2014, MNRAS, 441, 2663
Perley, D. A., Quimby, R. M., Yan, L., et al. 2016, ApJ, 830, 13
Petroff, E., Barr, E. D., Jameson, A., et al. 2016, PASA, 33, e045
Petroff, E., Johnston, S., Keane, E. F., et al. 2015, MNRAS, 454, 457
Pforr, J., Maraston, C., & Tonini, C. 2012, MNRAS, 422, 3285
Piro, A. L. 2016, ApJL, 824, L32
Planck Collaboration, Ade, P. A. R., Aghanim, N., et al. 2016, A&A, 594, A13
Schlafly, E. F., & Finkbeiner, D. P. 2011, ApJ, 737, 103
Schlegel, D. J., Finkbeiner, D. P., & Davis, M. 1998, ApJ, 500, 525
Scholz, P., Spitler, L. G., Hessels, J. W. T., et al. 2016, ApJ, 833, 177
Serra, P., Amblard, A., Temi, P., et al. 2011, ApJ, 740, 22
Spitler, L. G., Cordes, J. M., Hessels, J. W. T., et al. 2014, ApJ, 790, 101
Spitler, L. G., Scholz, P., Hessels, J. W. T., et al. 2016, Natur, 531, 202
Tendulkar, S. P., Bassa, C. G., Cordes, J. M., et al. 2017, ApJL, 834, L7
Thornton, D., Stappers, B., Bailes, M., et al. 2013, Sci, 341, 53
Thuan, T. X., & Martin, G. E. 1981, ApJ, 247, 823
van der Wel, A., Straughn, A. N., Rix, H.-W., et al. 2011, ApJ, 742, 111
Woosley, S. E. 2010, ApJL, 719, L204
Zaragoza-Cardiel, J., Font, J., Beckman, J. E., et al. 2014, MNRAS, 445, 1412
Zehavi, I., Blanton, M. R., Frieman, J. A., et al. 2002, ApJ, 571, 172